Aquat. Living Resour. 22, 447–461 (2009)

DOI: 10.1051/alr/2009054
www.alr-journal.org

Aquatic Living Resources

Evolution of upper layer temperature in the Bay of Biscay during the last 40 years

Sylvain Michel[1], Frédéric Vandermeirsch[1,a] and Pascal Lorance[2]

[1] Ifremer, département Dynamiques de l'Environnement Côtier, laboratoire de Physique Hydrodynamique et Sédimentaire, centre de Brest, BP 70, 29280 Plouzané, France
[2] Ifremer, département Études et Modélisation pour l'Halieutique, BP 21105, 44311 Nantes Cedex, France

Received 5 January 2009; Accepted 28 September 2009

Abstract – The temperature evolution over the past 40 years in the Bay of Biscay (North-East Atlantic) is investigated from an in situ data analysis, completed with a satellite SST (Sea Surface Temperature) analysis over the last 20 years. The in situ dataset is an interannual version of the BoByClim climatology, covering the Bay of Biscay area with a 10-km horizontal resolution and a 5-m vertical step. The satellite dataset is the European COastral Sea Operational Observing and Forcast System Program (ECOOP) daily analysis, covering the IBIROOS (Iberian-Biscay-Irish Sea) area with a 4-km resolution. The study area (43°N-50°N/12°W-1°W) extends over the intersection of the domains covered by these two analyses. In the 0–200 m layer of this domain, a heat budget has been computed from an ocean circulation model over the period 1965-2004. Heat is essentially imported from the west by the North Atlantic Drift, then exported southward and northward, or transferred downward into deeper layers. The annual average of air-sea flux is weak, with a zero isoline crossing the domain from the northwest to the southeast. Ocean and atmosphere, forming a coupled system, have comparable contributions and may both result in a heat sink or source. At the interannual scale, variability is mainly controlled by the air-sea flux, with a secondary contribution from oceanic transport. A strong warming of ~0.2 °C/decade for the period 1965-2004 is apparent from the surface down to the 200-m depth. The decadal evolution is consistent with several analyses over the North Atlantic. Meanwhile, warming is approximately twice faster than in the whole basin. This trend is not steady, as a cooling period occurred until the early 1970's, and the temperature increase has been significantly stronger during the last 20 years (~0.3 °C/decade between 0 and 100 m, from 1986 to 2005). The trend and the interannual variability are maximal over the northern part of the shelf. The typical duration of interannual anomalies is two years and their penetration depth is ~100 m, although they occasionally exceed 200 m. The interseasonal anomalies are also stronger within the mixed layer (root-mean-square, RMS = 0.6 °C at the surface) than below (RMS = 0.3 °C at 100 m). Their geographic distribution is radically different between the surface and the deep levels. A seasonal dependence of the warming rate is evident in the upper layer, as the temperature trend is stronger in summer than in winter (by a factor of 2 at the surface). Some of the potential implications for the ecosystem are discussed, particularly in terms of species distribution and dynamics of species exploited by fisheries.

Key words: Upper layer / Climatic change / Air-sea flux / Ocean circulation model / Satellite and in situ measurements / Ecosystem / Bay of Biscay

Résumé – L'évolution de la température durant les 40 dernières années dans le golfe de Gascogne (Atlantique Nord-Est) est étudiée à partir d'une analyse in situ, complétée par une analyse des températures de surface océanique (SST) issue de données satellitaires pendant les 20 dernières années. Le jeu-de-données in situ est la version interannuelle de la climatologie BoByClim, qui couvre le golfe de Gascogne avec une résolution horizontale de 10 km et un intervalle vertical de 5 m. Le jeu-de-données satellitaire est l'analyse journalière ECOOP, qui couvre la région IBIROOS (mers ibériques, golfe de Gascogne et mer d'Irlande) avec 4 km de résolution. La zone d'étude s'étend à l'intersection des domaines de ces deux analyses (43°N-50°N/12°W-1°W). Dans la couche supérieure (0–200 m) de ce domaine, un bilan thermique a été calculé à partir d'un modèle de circulation océanique sur la période 1965-2004. La chaleur provient essentiellement de l'ouest, apportée par la dérive Nord-Atlantique, puis est exportée vers le nord et le sud, ou transférée vers les couches inférieures. Le flux air-mer est faible en moyenne annuelle, avec une isoligne zéro traversant le domaine du nord-ouest au sud-est. L'océan et l'atmosphère, système couplé, ont des contributions comparables,

[a] Corresponding author: fvanderm@ifremer.fr

chacun pouvant constituer un puits ou une source de chaleur. A l'échelle interannuelle, la variabilité est principalement contrôlée par le flux atmosphérique, avec une contribution secondaire du transport océanique. Un fort réchauffement de ~0.2 °C/décennie pour la période 1965-2004 apparaît entre la surface et 200 m de profondeur. L'évolution décennale est cohérente avec plusieurs analyses dans l'Atlantique Nord. Cependant, le réchauffement est environ deux fois plus rapide que dans l'ensemble du bassin. Cette tendance n'est pas monotone, car elle inclut un refroidissement jusqu'au début des années 1970 et un réchauffement accéléré durant les 20 dernières années (~0.3 °C/décennie entre 0 et 100 m, de 1986 à 2005). La tendance et la variabilité interannuelle sont maximales dans la partie nord du plateau. La durée typique des anomalies interannuelles est de deux ans et leur profondeur de pénétration est de l'ordre de 100 m, mais dépasse parfois 200 m. Les anomalies inter-saisonnières sont également plus intenses dans la couche mélangée (racine de la moyenne des carrés, RMS = 0.6 °C) qu'en dessous (RMS = 0.3 °C à 100 m). Leur distribution géographique diffère radicalement entre la surface et les niveaux profonds. Dans la couche supérieure, le taux de réchauffement dépend de la saison, étant notablement plus fort en été qu'en hiver (d'un facteur 2 en surface). Certaines des implications potentielles pour l'écosystème sont discutées, notamment en termes de répartition et de dynamique des espèces exploitées par la pêche.

1 Introduction

Climate change is ongoing, whether its causes are anthropic or natural, and is modifying the environment of marine ecosystems. Part of the ocean warming observed during the last decades is attributable to natural fluctuations, such as the Atlantic Multidecadal Oscillation, which may modulate human-induced changes in the future (Knight et al. 2005). Warming affects the whole northern hemisphere, particularly the North Atlantic (Curry and Mauritzen 2005; Levitus et al. 2005). However, strong regional modulations of temperature changes have been evidenced. From 1950 to 2000, the subtropical North Atlantic has warmed and the subpolar part has cooled, with a separation line at about 40°N close to the eastern boundary (Lozier et al. 2008). More recently, from 1999 to 2005, the eastern North Atlantic subtropical regions (south of 40° N) have been cooling, while subpolar regions (north of 50° N) have been warming (Ivchenko et al. 2006). Thus, the Bay of Biscay is located within the area of transition between warming and cooling areas. Moreover, the geographical limit of this transition has likely moved considerably during the last decades. The studies cited above address interannual temperature change at the scale of the whole North Atlantic basin. Few studies are dedicated to the regional scale of the Bay of Biscay. Nonetheless, some authors concluded that the sea surface of the area had warmed between the 1970s and 1990s, particularly in its southeastern corner (>0.6 °C/decade) (Koutsikopoulos et al. 1998; Planque et al. 2003). However, their findings lack robustness as their datasets were limited to the surface layer and to a time period too short for climatic scales.

The present study focuses on the temperature evolution in the Bay of Biscay within the upper 200-m layer. The study area includes shelf seas (Cantabrian, Aquitaine, Armorican and Celtic shelves) as well as deep ocean areas (down to 5000 m). In these regions, temperature in the upper and intermediate layers has been measured regularly since the 1960s, using in situ instruments. Sea surface temperature (SST) has been monitored at high resolution and frequency by satellite remote sensing since the mid-1980s. Additionally, ocean circulation models enable understanding the mechanisms of temperature variability. Here, we combine all three types of information to study temperature evolution over the past 40 years at interseasonal, interannual and decadal time scales. Another study (Michel et al. 2009) is dedicated to the analysis of temperature interannual variations in this region and during the same period over a deeper layer (0–800 m). This previous study has shown that the warming trend culminates to 0.23 °C/decade at 50 m and remains positive down to about 500 m. In the present study, we focus on shallower waters, whose conditions have more direct consequences on human activities (e.g. fishing) and where seasonal variations are of a much larger amplitude, making their estimation essential. It is stressed that the datasets used in this study are different and at a higher resolution, both in time (season or month instead of year) and space (about 0.1° in longitude and latitude, instead of 0.25°), from those in Michel et al. (2009).

After introducing the topic, the observational datasets and the numerical simulation are described first, then the statistical quantities applied to these datasets are defined. Then, possible causes of observed temperature changes and anomalies are investigated based upon the model simulation and the interannual evolution, including decadal trends and annual anomalies, is quantified. The spatial distribution of SST variations is described in detail using satellite data, their spread into deeper water is examined from in situ temperature data and seasonal and interannual anomalies are investigated. Finally, some of the implications for marine ecosystems are discussed and the main results are summarised.

2 Data and methods

2.1 Datasets

2.1.1 Satellite SST

The satellite SST data are obtained from Advanced Very High Resolution Radiometer (AVHRR) remote sensing of the sea surface infra-red emission. These data are available from the NOAA series satellites since 1985. An analysis was performed during the European COastral Sea Operational Observing and Forecast system (ECOOP) programme over the IBIROOS area (30°N-60°N and 12°W-12°E, Fig. 1), providing daily fields from 1986 to 2006, at a spatial resolution of 0.044° (~4 km) (Saulquin and Gohin 2009). The ECOOP product has been generated by Saulquin and Gohin (2009) using the following method. First, an empirical model is determined at each point, using all good quality data. Second, deviations from this model are kriged (through an optimal interpolation) in order to fill data gaps over the whole area and for all days within the period. This method results in homogeneous SST fields, which are almost free of missing data associated with clouds and extend very close to coasts.

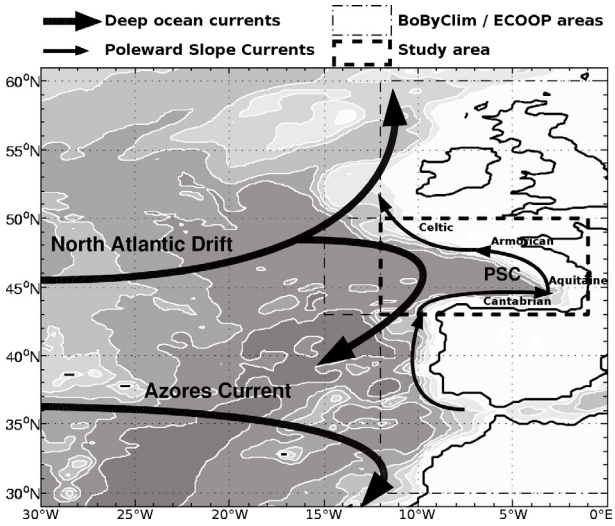

Fig. 1. Bathymetric map and main circulation features in the upper layer (0–200 m) of the NE Atlantic (continental shelves (<200 m) in white; depth contours every 1000 m).

2.1.2 Global analysis of in situ temperature

For reference purposes, we use the interannual analysis of temperature in the global ocean by Levitus et al. (2005). This analysis is based on the World Ocean Database (WOD), consisting of measurements from all kinds of instruments, which were collected and archived by the National Oceanographic Data Center (NODC). These data were interpolated, using an objective analysis technique, onto a regular 2D grid with a 1° spatial resolution (~110 km at the latitudes of the Bay of Biscay). Annual fields were produced from 1955 to 2003, on vertical levels separated by 10 to 200 meters, from the surface down to 700 m.

2.1.3 Regional analysis of in situ temperature

Our main in situ dataset is the BoByClim analysis (Vandermeirsch et al. 2008), dedicated to the Bay of Biscay. This analysis includes the WOD data in this region (35% of the dataset), as well as numerous eXpendable BathyThermographs (XBT) profiles from Service Hydrographique et Océanographique de la Marine (SHOM, French Navy, 46% of the data) and additional measurements from Ifremer (17% of the data). Thus, its data density is much higher than in WOD and covers a slightly longer period (1950 to 2005). It is produced using an optimal interpolation technique similar to that of Levitus et al. (2005). The main difficulty in generating this hydrological atlas consists in representing both the coastal scales on the shelf and the deep ocean scales over the abyssal plain. This problem is addressed by varying the influence radius, the key parameter in the objective analysis, as a function of bathymetry. The analysed area spreads from 43°N (northern Spanish coast) to 50°N (central Celtic Sea) and from the French coast (about 1°W) to 15°W (Fig. 1), at a 1/10° spatial resolution corresponding to about 10 km. The temperature data is interpolated at depth levels set every 5 m from the surface down to 50 m, then every 10 m down to 200 m. The analysis is performed both at the annual scale and seasonal scale (every 3 months) from 1950 to 2005.

2.1.4 Ocean circulation model

Because of the lack of current velocity measurements at the scales of interest, we used a 3D circulation model to estimate oceanic transport of heat. We chose the ORCA025-G70 simulation, designed within the DRAKKAR project (Barnier et al. 2006, http://www.ifremer.fr/lpo/drakkar/) and based on the NEMO (Nucleus for European Modelling of the Ocean) deep-ocean model. The horizontal grid covers the global ocean with 1/4° resolution (~25 km in the Bay of Biscay) and the vertical grid consists in 46 levels, whose thickness increases with depth from 6 to 200 m. The simulation was run from 1958 to 2004, after a 7-year spin-up phase, using realistic daily fluxes to force the ocean surface (Brodeau et al. 2007). These fluxes (of heat, fresh water and momentum) are computed using state-of-the-art parameterisations (Large 2007). The meteorological fields are outputs from the ECMWF model (ERA40 reanalysis), whereas precipitations and solar radiation are obtained from satellite data.

We extracted the simulated temperature, air-sea fluxes and current velocity data at every grid points and at all depth levels within our study domain. The model time step is one hour and outputs are averaged and saved every five days. We use annual averages of the simulated variables, as we focus on their interannual variations.

2.2 Methods

2.2.1 Statistics

To extract relevant information from these large datasets, some basic statistic calculations were applied, focusing alternatively on temporal evolution, spatial distribution or vertical variation within the 0–200 m layer:

- A "layer average" is determined vertically from the surface down to 200 m (or less, if the seafloor is shallower, e.g. over the continental shelf).
- An "area average" is determined horizontally over the Bay of Biscay domain, defined as the intersection of the ECOOP and BoByClim areas (43°N-50°N / 12°W-1°W, Fig. 1).
- A "domain average" is a 3D average, obtained from a horizontal averaging combined with a vertical averaging. Note that the domain heat content (HC) is proportional to the domain averaged temperature ($\overline{\overline{\overline{T}}}$):

$$HC(t) = C_p \rho_0 V \overline{\overline{\overline{T}}}(t) \quad (1)$$

where C_p = 4200 J kg^{-1} K^{-1} (joule per kg kelvin) is the specific heat of seawater, ρ_0 = 1020 kg m^{-3} is the reference density of seawater and V is the domain volume.

The "linear trend" is obtained by fitting a time series to a straight line (through a least-square linear regression). Applied to a temperature time series, this quantity represents the mean

rate of change, e.g. climatic warming (or cooling) in a given domain. Additionally, the "residuals" are obtained by subtracting the linear trend from the original time series. Decomposing a series into its trend and residuals is the simplest way of separating time scales, by removing the slow evolution (trend) from faster fluctuations (residuals):

$$T(t) = \hat{T} + T'(t) = \hat{T} + Lt + T''(t)$$
$$\hat{T} = \frac{1}{N}\sum_{t=1}^{t=N} T(t), \sum_{t=1}^{t=N} T'(t) = \sum_{t=1}^{t=N} T''(t) = 0 \qquad (2)$$

where N is the number of time-steps, $\hat{T}$ is the time mean, $T'(t)$ are the anomalies, L is the linear trend and $T''(t)$ are the residuals.

Alternatively, an interannual time-series can be decomposed into its variations at seasonal and annual scales:

$$T(t) = T(y,s) = \hat{T} + T'_{\text{annual}}(y) + T'_{\text{seasonal}}(s) + T''_{\text{interseasonal}}(y,s) \qquad (3)$$

where y is the year number, s is the season number, $T'_{\text{annual}}(y)$ is the annual anomaly, $T'_{\text{seasonal}}(s)$ is the mean seasonal cycle and $T''_{\text{interseasonal}}(y,s)$ is the anomaly from the seasonal cycle. Note that s ranges from 1 to 4 in case of a quarterly means (as in the BoByClim interannual analysis) and from 1 to 12 in case of monthly means (as from the ECCOP daily analysis).

The "standard deviation" is the root-mean-square of a time series. It can be applied to anomalies, to residuals, to differences between two series, to a series of annual mean values (interannual standard deviation), to the mean seasonal cycle, etc.

The "temporal correlation" is the coefficient of correlation between two time series.

The "empirical orthogonal functions" (EOF), also called "principal component analysis", are the decomposition of a time-evolving field into stationary patterns. Each EOF represents a part of the total signal variability, called "explained variance" and usually expressed as a percentage of total variance. A time series of coefficients is associated with each EOF, indicating the modulation of the corresponding pattern as a function of time (including sign reversals).

2.2.2 Thermal balance

The "thermal balance" (or "heat budget") is a quantification of the sources and sinks of heat within a fixed 3D domain. Here, we consider a domain as a rectangular box for the sake of simplicity. Our study domain (Fig. 1) is limited by three lateral open boundaries in the south (at 43°N), west (at 12°W) and north (at 50°N). The eastern limit and part of the southern limit are closed by coasts. The domain is also limited by two vertical boundaries: the sea surface and the 200-m depth level. The heat budget is computed from model outputs, as observed data are generally too sparse in time and space to estimate properly all the budget terms.

At each grid point, the local heat budget can be written as a sum of terms, with the dimension of a heat transport (in joule s^{-1} or watt). The heat content (HC) variations can be simply expressed as the sum of three terms: the air-sea flux at the surface (HT_A), the sum of oceanic transports across each boundary (HT_T) and the heat diffusion (HT_D) (accounting for turbulent mixing, eddies and currents with typical sizes smaller than a few grid cells). Thus, the budget is reduced to:

$$\partial HC/\partial t(x,y,t) = HT_A(x,y,t) + HT_T(x,y,t) + HT_D(x,y,t). \qquad (4)$$

The role of each term in the thermal balance can be quantified through its mean amplitude (A_i), representing its impact on local temperature variations. The ratio of this amplitude with respect to the sum of all amplitudes (P_i) indicates the "contribution" of this term to temperature variability. For example, in the case of the air-sea heat flux, the amplitude (in watt) and the contribution (in percent) can be written:

$$A_A(x,y) = \frac{1}{N}\sum_{t=1}^{t=N} |HT_A(x,y,t)|$$
$$P_A(x,y) = 100\frac{A_A(x,y)}{A_A(x,y) + A_T(x,y) + A_D(x,y)}. \qquad (5)$$

Then, the thermal balance at each grid point can be summarised by the contribution P_A, P_T and P_D. These 3 contributions can be plotted on a single map by allocating P_A, P_D and P_T to the red, green and blue components of the colour at each pixel.

3 Results

3.1 Thermal balance in the 0–200 m layer

3.1.1 Mean thermal balance

We first describe the simulated thermal balance computed from the ORCA simulation for the period 1965-2004 (Fig. 2). On average, the atmosphere contribution is close to zero: the mean over the 40-year period of the air-sea flux (HT_A) is +0.3 TW (1 terawatt, i.e. 1 TW = 10^{12} watt). The heat input associated with river runoffs, precipitations and evaporation is weaker (mean = +0.08 TW). The heat input associated with the rising sea level is even weaker by one order of magnitude (mean = +0.01 TW). In addition, the two latter heat inputs exhibit weaker variations (std. dev. < 0.1 TW) than the air-sea flux, and the local contribution of the freshwater flux (E-P-R) is negligible out of littoral and estuarine areas. As a consequence, the impacts of sea level rise and freshwater flux on the heat balance can be neglected at the domain scale.

The main heat input comes from the transport across the western boundary (mean = +22 TW), as an extension of the North Atlantic Drift (NAD) brings warm water into the domain (Fig. 1). The NAD is a wide current flowing eastward through the North Atlantic, from the Gulf Stream to the European shelf seas, that splits into a northward and a southward branch while approaching the continental margin. The NAD southern branch is responsible for the main heat output (mean = −14 TW) from the domain. Note that the Iberian Poleward Current (IPC), i.e. the southern part of the Poleward Slope Current, brings warmer Mediterranean water northward.

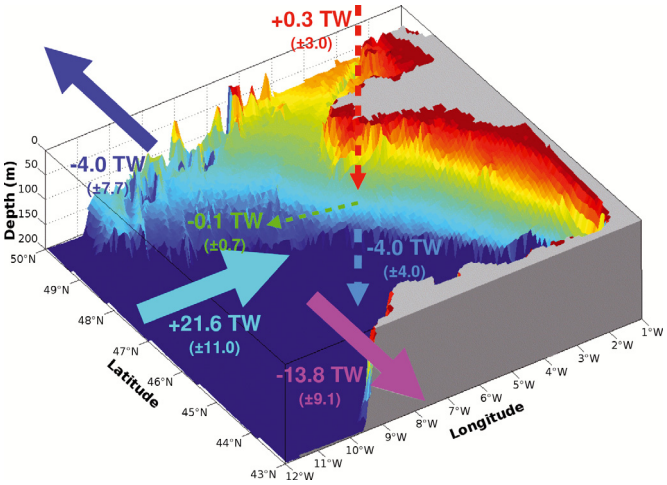

Fig. 2. Thermal balance in the 0–200 m layer averaged over the 1965-2004 simulation. Coloured 3D surface: bathymetry in the 0–200 m range. Arrows: heat inputs/ouputs in terawatt (TW, 10^{12} watt) with standard deviations in brackets (see text).

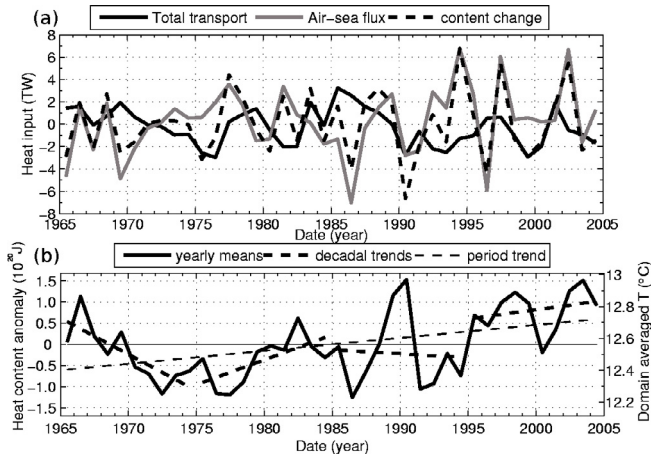

Fig. 3. (a) Interannual evolution of the heat budget in terawatt (TW, 10^{12} watt) in the 0–200 m layer. (b) Interannual anomaly of the heat content (in 10^{20} joules) and corresponding domain-averaged temperature (right axis, in °C).

But as its core is located deeper than 200 m (Friocourt 2007), its impact in the 0–200 m layer is secondary. A weaker heat export takes place across the northern boundary (mean = −4 TW), attributed to the Celtic slope current.

Note that these results depend on the domain limits, but they are fairly robust when displacing the boundaries by a few degrees (Michel et al. 2009). For instance, when moving the western boundary toward the eastern coasts, the westerly import is reduced but remains the main source of heat into the domain. In parallel, the northward export diminishes and the southward export switches to a heat import.

The vertical currents export heat downward into the deeper layer, below 200 m, (mean = –4 TW) and approximately compensate the heat input by horizontal currents. As a result, the sum of horizontal and vertical heat transports is only slightly negative (mean = –0.2 TW). The difference between the heat input by air-sea flux (HT_A = +0.3 TW) and the heat loss by oceanic transports (HT_T = −0.2 TW) is due to heat diffusion (HT_D = −0.1 TW). Coincidentally, the sum of all these terms is close to zero for this particular period because the heat content is almost the same at the beginning (t_0 = 1 January 1965) and at the end (t_1 = 31 December 2004) ($HC(t_0) \approx HC(t_1) \approx 4.72 \times 10^{21}$ joules). However, this does not imply that the heat content remains stable over the whole period.

3.1.2 Interannual evolution of the thermal balance

We now consider how the thermal balance varies from year to year during the period 1965-2004 (Fig. 3a). The air-sea flux is the major source of interannual variability (std. dev. = 3.0 TW). In comparison, the variability of oceanic heat transport (horizontal + vertical) is about twice lower (std. dev. = 1.6 TW) and heat diffusion variability is much weaker (std. dev. = 0.7 TW). The variability of annual heat content change (std. dev. = 1.9 TW) is comparable to that of the air-sea flux and oceanic transport. The heat content variations are strongly correlated to the air-sea flux (correlation = 79%, significant at more than 99%). As explained previously, the heat content is proportional to the temperature averaged in the 3D domain, whose annual variations are displayed (Fig. 3b).

In terms of linear trends, the air-sea flux tends to increase over 40 years (trend = +0.6 TW/decade), while the total oceanic transport tends to become more and more negative (trend = –0.3 TW/decade). The air-sea heat flux is significantly negative during the first decade (mean = –0.9 TW), then increasingly positive with frequent sign reversals during the second and third decades, and generally positive during the last decade (mean = + 1.1 TW). In contrast, the total transport is positive during the first decade (mean = + 0.4 TW), then predominantly negative, especially during the last decade (mean = –0.7 TW). The air-sea heat flux and the total transport are markedly anti-correlated (–34%, significant at 97%). The compensation between these two terms may be attributed to the atmosphere-ocean system coupling.

The domain heat content tends to decrease during the first decade (cooling trend of –0.5 TW) (Fig. 3b). Then, the heat content increases rapidly during the second decade and remains almost unchanged during the third decade. Warming starts again during the last decade, at a rate equivalent to the whole period average: a heat content trend by 0.1 TW. Over the whole 40-year period, the heat content trend becomes more and more positive (from –0.5 to + 0.1 TW) and the upper layer warming accelerates during the last decades.

3.1.3 Air-sea heat flux

We consider separately the atmospheric component of the thermal balance in the domain. The mean air-sea heat flux exhibits a much contrasted geographical distribution over the Bay of Biscay area (Fig. 4a). Over the period 1965-2004, its mean value ranges between –20 W m^{-2} to the north of Brittany and +30 W m^{-2} to the west of Galicia. The heat flux is positive to the northwest of Spain, as far north as 47.5°N, while it is negative further north and in the interior Bay of Biscay,

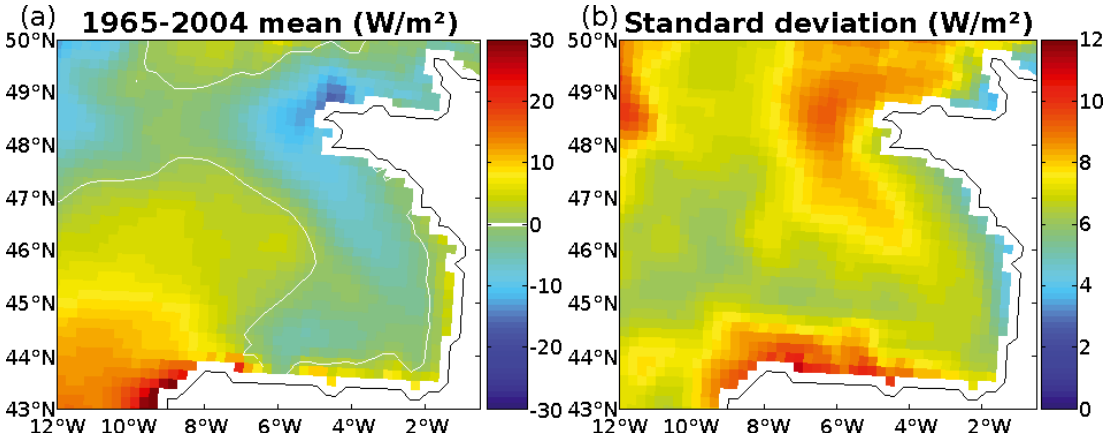

Fig. 4. (a) Mean net air-sea heat flux from the 1965-2004 simulation. (b) Interannual standard deviation of net heat flux.

roughly east of 6°W. Low positive values are also found in the northern Celtic Sea, as well as along a coastal fringe, south of the Loire estuary (47°N). The seasonal cycle of the air-sea heat flux has a strong amplitude (up to ±200 W m^{-2}), mainly due to variations in solar heating (not shown).

The flux has a marked temporal trend towards higher values over the whole area, particularly offshore northern Spain, and its zero isoline tends to shift with time toward the north and east of the domain (not shown). This results in an atmospheric warming spreading inside the Bay of Biscay, except the Armorican shelf.

The interannual variability of the air-sea heat flux is also heterogeneous (Fig. 4b). The variations are stronger along the Cantabrian Sea (10 W m^{-2}) and over the Armorican shelf (8 W m^{-2}), as these two regions are respectively exposed to intense winds and variable cloud conditions. Conversely, the variability is weakest along the French coasts (down to 5 W m^{-2}), except northern Brittany, where the wind is generally lower and the meteorological conditions steadier. Note that uncertainties on the mean values of air-sea heat fluxes are probably of the same order of magnitude as their interannual variability (~10 W m^{-2}). Indeed, sensitivity experiments carried on using a global ocean model result in ±10 W m^{-2} biases on the mean net heat flux in this region (Brodeau et al. 2007). The Bay of Biscay area is particularly sensitive to the air-sea flux estimates, as its spatial average is close to zero (integral of +0.3 TW over the period, equivalent to a mean flux of +0.1 W m^{-2}). Thus, the sign of the air-sea flux long-term mean is uncertain over the study area, but its spatial and interannual variability is large enough to be captured by the simulation.

3.1.4 Relative contributions of atmosphere, ocean circulation and mixing

We use the simulated heat budget evolution to quantify the causes of temperature interannual variations. The amplitudes of heat changes associated with the three major processes are computed and compared using a trichromatic color scale (Fig. 5). For example, a purple square signifies that in this grid cell, interannual heat content variations are caused at 50% by air-sea flux and at 50% by oceanic transport; a turquoise square: 50% by oceanic transport and 50% by diffusion; a yellow square: 50% by air-sea flux and 50% by diffusion. All intermediary combinations of two or three terms are possible.

Air-sea flux appears important over most of the domain and is generally combined with oceanic transport. Oceanic transport dominates along the French coastal fringe, where air-sea flux is low and weakly variable (Fig. 4). Oceanic transport and diffusion dominate along parts of the continental slope, particularly in the Cantabrian and Basque seas, as well as in the western Celtic Sea. Diffusion alone (accounting for small scale circulation and mixing) is the major term along the coast of southern Brittany, where both the annual mean flux and the permanent currents are low. Thus, the interannual variability of temperature in the 0–200 m layer is rarely governed by a single process, but more often by a combination of atmospheric and oceanic processes.

3.2 Temperature interannual variations

3.2.1 Temporal evolution at the surface and at depth

The temperature variations in the domain are examined in details by focusing on fixed depths, rather than on the 0–200 m layer (Fig. 3b). In the following sections, we base our study on the temperature observations (BoByClim and ECOOP analyses), instead of the simulated temperature, to take advantage of their higher resolution. Note that the area averaged temperatures from the simulation and from the observations are fairly consistent (Michel et al. 2009). We can therefore rely on the thermal balance inferred from the simulation. The WOD analysis was also used to validate the high-resolution datasets and check their consistency. For instance, the correlation between BoByClim and WOD, in terms of temperature averaged horizontally and annually from 1965 to 2003, is higher than 90% in the whole layer. Also the mean difference between these two analyses is lower than +0.15 °C and its standard deviation is lower than 0.18 °C, both of which decrease with depth.

At the surface (Fig. 6a), strong year-to-year temperature fluctuations are superimposed on a clear warming trend. The domain averages of the ECOOP SST and of the BoByClim temperature at 5 m are correlated to 92%, a result which

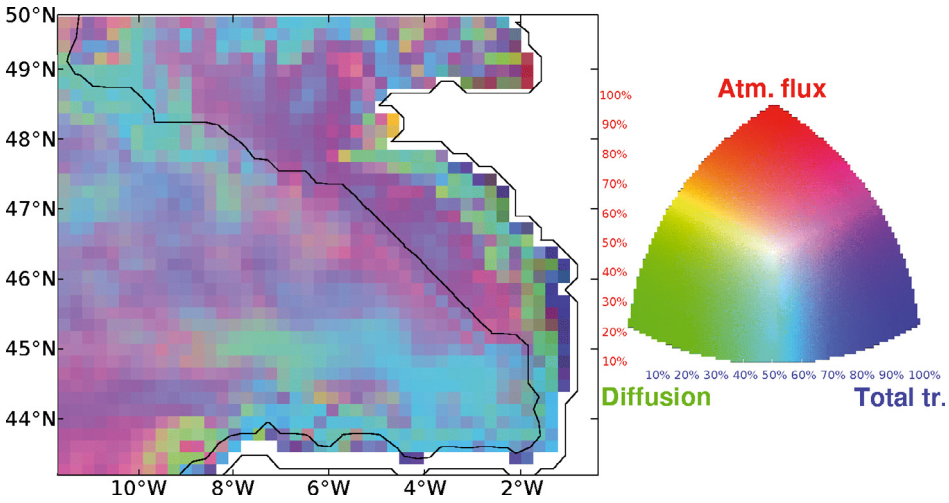

Fig. 5. Relative contributions of the three major terms to the interannual thermal balance in the 0–200 m layer from the 1965-2004 simulation (see text). Black contour: 200 m isobath.

confirms the robustness of these temperature estimates. Over the period 1965-2003, the standard deviation in BoByClim amounts to 0.44 °C. Over the last 20 years, BoByClim exhibits stronger variations (std. dev. = 0.47 °C) than during the whole period, while the ECOOP satellite data has a slightly lower variability (std. dev. = 0.41 °C). The 40-year trend is estimated to +0.24 °C/decade in BoByClim. The trend is significantly higher during the last 20 years: +0.30 °C/decade in BoByClim, slightly below the warming rate from the ECOOP analysis: +0.36 °C/decade. The variability of residuals also increases during the last 20 years (std. dev. from 0.28 to 0.44 °C for BoByClim). Thus, not only the decadal trend but also year-to-year variations are higher during the second half of the period.

Because the 50 m level (Fig. 6b) is generally located within the seasonal mixed layer, its temperature variability and trend are similar to those of SST. The standard deviation is only slightly lower than at the surface: 0.40 °C. In contrast, the linear trend is slightly higher than at the surface: 0.28 °C/decade. Thus, a larger part of variability is due to slow (i.e. multi-decadal) change compared to faster (i.e. year-to-year) fluctuations. The 200-m level (Fig. 6c) is situated at the base of the seasonal thermocline, thus the temperature at 200 m is partially isolated from the effect of air-sea heat flux variations. The standard deviation is about half its surface value: 0.23 °C. The warming trend is still significant, although lower than above: 0.15 °C/decade.

Note that the trends are not uniform during the 40-year period (Fig. 3b): there is a decrease in temperature until 1977-78, then an increase during the rest of the period, with a faster warming from 1995 onward. In the upper layers, the temperature minimum is reached around 1972, thus the cooling phase ends sooner and the warming phase lasts longer. Therefore, warming starts at or close to the surface in the early 1970s, then slowly penetrates, reaching the 200 m depth level after about five years. The trend values are significantly higher than the warming rate estimated for the 0–300 m layer in the whole North Atlantic (Levitus et al. 2005: +0.08 °C/decade over the 1955-2003 period). Their analysis shows a slight decrease of temperature during the 1960s, followed by a strong increase

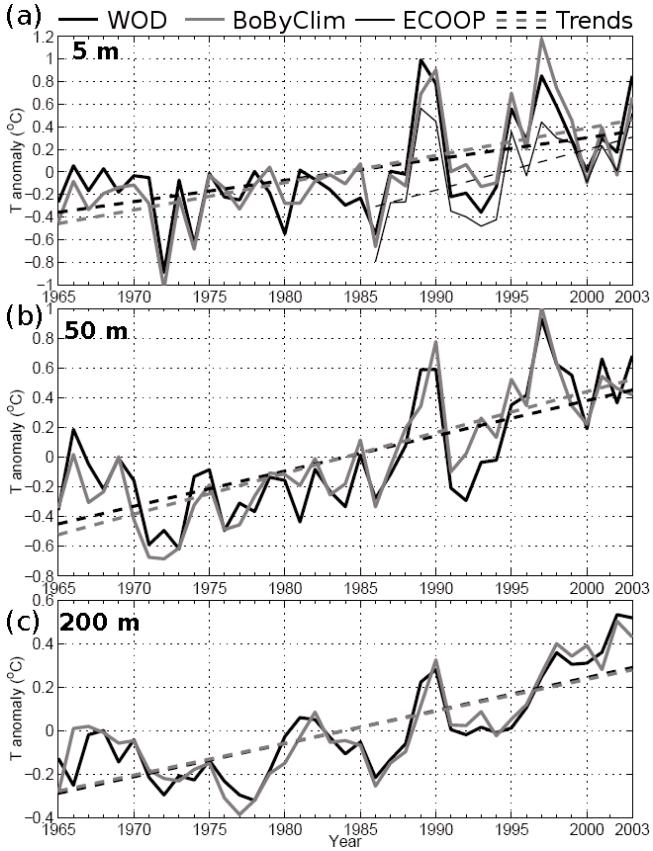

Fig. 6. Interannual anomalies of temperature averaged over the domain area (43°N-50°N, 12°W-1°E), at three different depths: (a) 5 m, (b) 50 m and (c) 200 m.

starting from the early 1970s. As a consequence, the long-term evolution of temperature in the Bay of Biscay is similar to those of the North Atlantic, although with a few years' delay and an enhanced magnitude.

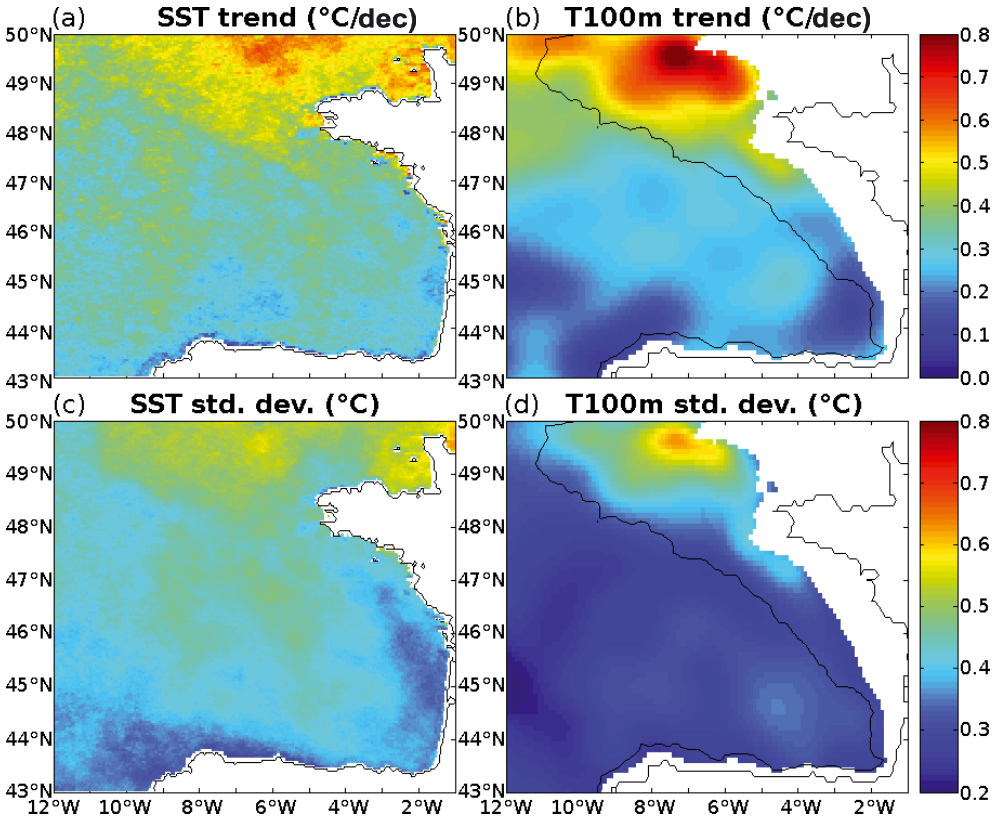

Fig. 7. Temperature interannual variability during 1986-2005: linear trend of (a) SST from ECOOP and (b) temperature at 100 m from BoByClim; interannual standard deviation of (b) SST from ECOOP and (d) temperature at 100 m from BoByClim. Black contour in (b) and (d): 200 m isobath.

3.2.2 Geographic distribution of interannual variability

The ECOOP and BoByClim datasets reveal that variability is far from uniform within the Bay of Biscay. At the surface (Fig. 7a), the satellite SST shows that the warming trend is highest over the northern Armorican shelf, where the trend reaches 0.6 °C/decade. This value is consistent with the study of the English Channel based on the same SST analysis (Saulquin and Gohin 2009). The trend is also high over the whole Celtic and Armorican shelves, except to the south of 47°N. The warming is much lower elsewhere, about 0.3 °C/decade in the southern part of the Bay of Biscay. The BoByClim temperature at 5 m (not shown) confirms this general northeastward gradient, with even higher values over the northern Armorican shelf (up to 1.0 °C/decade).

At the surface, the interannual variability exhibits approximately the same distribution as the linear trend (Fig. 7c). A high standard deviation is found over most of the Armorican shelf (about 0.5 °C). The values are much lower in the Ushant Front and Iroise Front areas, where strong permanent mixing by tidal currents impedes temperature variations from one year to another. The variability is particularly weak (0.3 °C) over the Aquitaine and Cantabrian shelves, extending offshore to the west of Galicia. Note that the distribution of interannual variability differs markedly for temperature (Fig. 7c) and for air-sea heat flux (Fig. 4b). This indicates that the surface temperature evolution is not governed by atmospheric processes alone, as we concluded from the simulated thermal balance in the 0–200 m layer (Fig. 5). The BoByClim analysis overall confirms the pattern from ECOOP (not shown), but also shows a high variability in the coastal fringe of the south-eastern sector, probably because of data sampling issues.

At 100 m (Fig. 7b), the linear trend is also positive everywhere in the domain. A clear maximum (0.8 °C/decade) is found over the northern Armorican shelf as a projection of the surface maximum (Fig. 7a). The trend is much weaker over the abyssal plain (lower than 0.4 °C/decade), particularly in the southeastern corner (Basque Sea) and offshore Galicia, but warming remains significant everywhere.

At this depth also, the distribution of standard deviation (Fig. 7d) is similar to that of the linear trend, with a maximum around the same location (up to 0.6 °C). The variability is high over the whole Celtic shelf, as well as over the shallowest part of the Armorican shelf. It is almost uniform inside the Bay of Biscay, with values about 0.3 °C everywhere to the east of 10°W and slightly higher (0.35 °C) over the southeastern abyssal plain. Therefore, the main features of warming and fluctuations are roughly similar in the upper 100 m, with the strongest interannual variations taking place over the Armorican shelf.

3.2.3 Horizontal patterns of interannual variability

The stationary patterns of interannual variability are revealed by the empirical orthogonal functions (EOF)

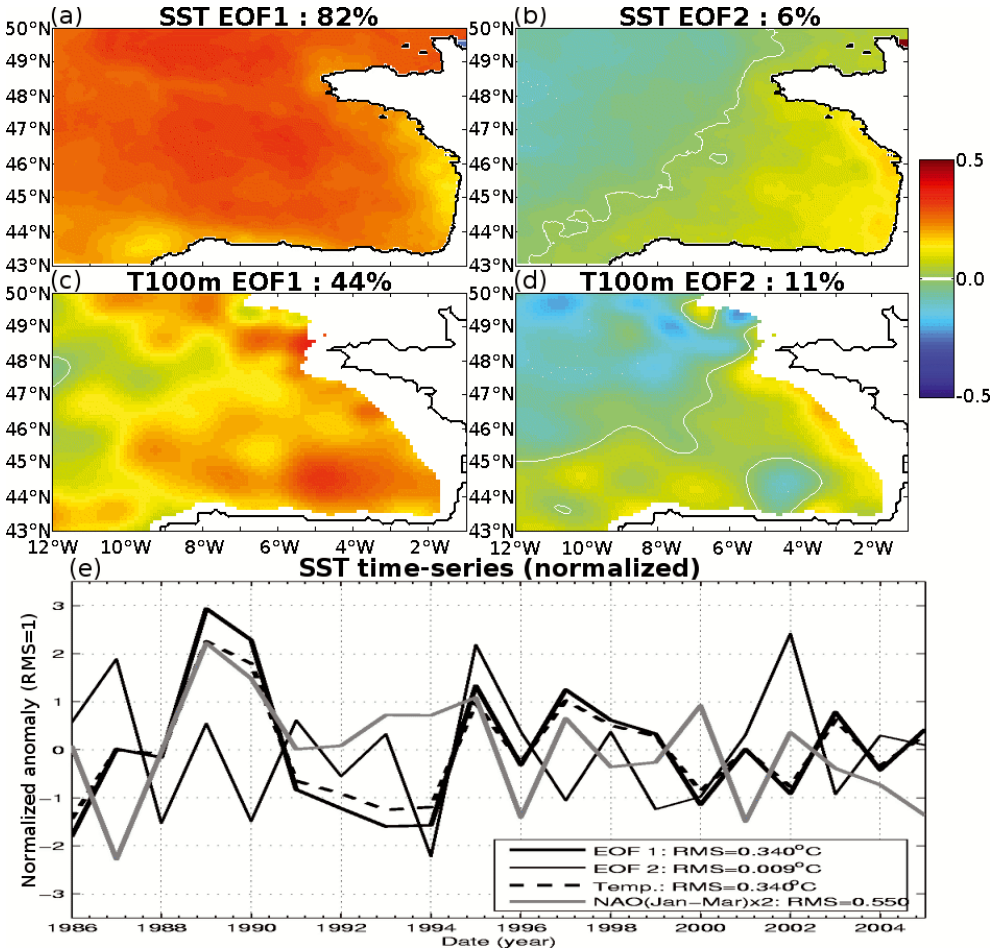

Fig. 8. EOFs of temperature interannual residuals during 1986-2005 (in °C). (a) EOF1 and (b) EOF2 from the ECOOP SST; (c) EOF1 and (d) EOF2 from the BoByClim temperature at 100 m. The explained variance (in %) is indicated above each panel. (e) Normalized SST time-series (std. dev. = 1) of EOF1 and EOF2 compared with the SST total residuals and the NAO index in winter (i.e. January to March average; index × 2).

decomposition of annual mean temperature fields. Thus, time scales below two years are filtered out. We use annual residuals, rather than annual anomalies, to remove the influence of trend.

At the surface, the first EOF (EOF1) is almost uniform over the Bay of Biscay area (Fig. 8a), as its amplitude ranges between 0.2 and 0.3 °C everywhere (mean = 0.26 °C). This pattern is largely dominant and explains 82% of the interannual variance. The second EOF (EOF2) represents 6% of the interannual variability and its amplitude is much weaker (mean = 0.06 °C). In contrast with EOF1, however, EOF2 consists in a northwest/southeast gradient (Fig. 8b), with one pole concentrated along the Aquitaine shelf and Landes Plateau, while the other pole is spread over the northwestern sector. In the BoByClim analysis at 5 m (not shown), EOF1 and EOF2 exhibit similar patterns as in ECOOP, but they are associated with a lower explained variance. Thus, in the in situ analysis, interannual variability is distributed into a larger number of modes.

At the 100 m depth, EOF1 from the BoByClim analysis represents 44% of the interannual variability. Its pattern is still single-signed (Fig. 8c), but a pole of intensified amplitude is located in the Cantabrian Sea. The distribution of EOF2 (Fig. 8d) is close to that of the satellite SST (Fig. 8b), dominated by a northwest/southeast opposition, with an elongated eastern pole against the shelf-break and a diffuse western pole over the abyssal plain. This mode is more significant than in the SST, as it explains more of the variance (11%), and its mean amplitude is similar (mean = 0.07 °C). Therefore, while the interannual variations of surface temperature can be summarised by a single mode, they become more complex at a greater depth.

The North Atlantic Oscillation (NAO) is the first mode of atmospheric variability over the whole basin. The NAO index is defined by the surface pressure difference between the Azores region and Iceland, usually most intense in winter. The winter NAO index is compared to the time series of the main SST interannual modes (i.e. EOF1 and EOF2) (Fig. 8e). As expected from the percentages of explained variance, the EOF1 time series is almost superimposed on the SST residuals, while EOF2 modulates the SST variations. The time series of EOF1 is significantly correlated to the NAO index (29%) and this correlation increases when considering the SST in winter (41%, not shown). Note that the correlation between EOF1 and the NAO increases when considering a larger area

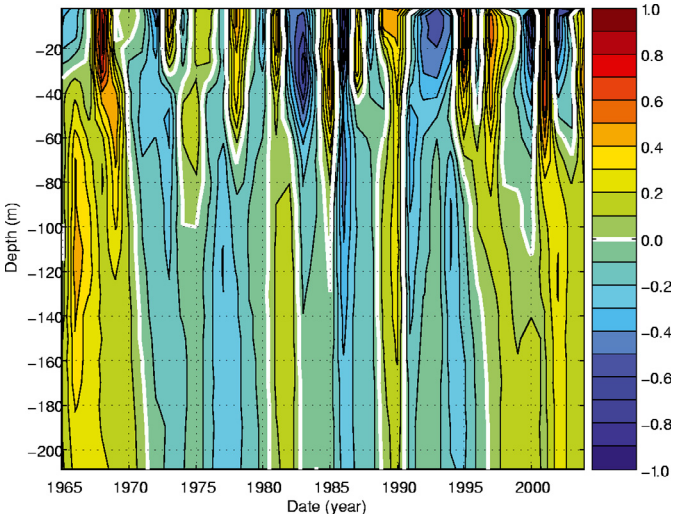

Fig. 9. Time/depth diagram of temperature interannual residuals (in °C) from BoByClim, averaged horizontally over the study area.

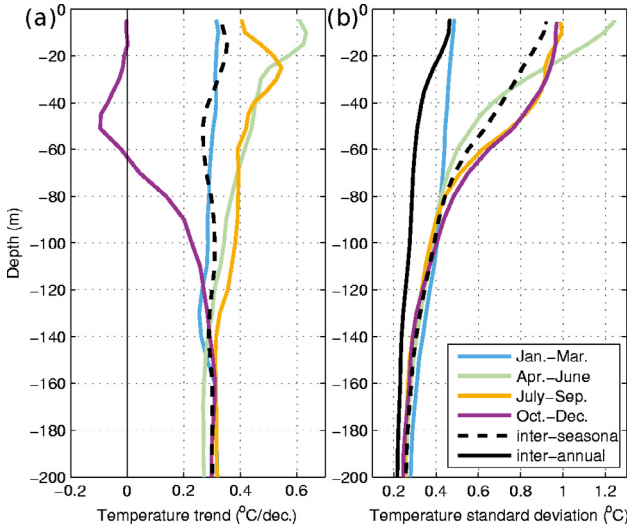

Fig. 10. Vertical and seasonal distribution of temperature interannual variability from BoByClim (1986-2005), averaged horizontally over the study area: (a) linear trend; (b) standard deviation of seasonal anomalies. Dashed black line: mean of four seasons. Black line in (b): std. dev. of interannual anomalies.

(Michel et al. 2009). Moreover, EOF1 has a large-scale pattern, suggesting it could originate from atmospheric variability. Therefore, the dominant mode of SST interannual variability in this region (EOF1) seems to be related to the major mode of atmospheric variability over the whole North Atlantic (i.e. the NAO). The same conclusion is reached when using the in situ temperature from BoByClim at any depth between 5 and 200 m (not shown). A more detailed analysis would be required to understand the mechanisms linking the Bay of Biscay upper layer temperature and the NAO, for instance by using seasonally varying fields instead of annual mean fields.

3.2.4 Vertical distribution of interannual anomalies

Here, the vertical distribution of the temperature anomalies is described (Fig. 9) to capture the connection between observations at selected depth levels (Fig. 6). Despite the removal of the trend over the 40-year period, a cooling phase is clearly seen until the mid 1970s, followed by a slower warming phase during the last 30 years. Thus, the trend over the whole period is not representative of the decadal evolution of temperature. Moreover, the slow temperature variations are frequently modulated by cool and warm anomalies, with a typical duration of ~2 years.

Most anomalies are enhanced at the surface or in the top layer, but a few exhibit a core at depth. For example, the 1966 warm anomaly has its maximum at about 120 m, and the 1991-1994 cool anomaly starts at 60 m. The strongest anomalies penetrate down to 200 m or more, such as the 1986 cool event and the 1989 warm event. During the last decade, warm anomalies are more sustained, so that warming penetrates deeper and deeper from one year to the next. For instance, the warm anomaly starting at the surface in 1995 reaches the 200 m depth in 1997, then the layer below 100 m remains anomalously warm. The duration and vertical extent of each anomaly are controlled by the competition between the air-sea fluxes (forcing or attenuating anomalies at the surface) and oceanic currents (importing anomalous water masses or transporting then away and deeper) as seen from the thermal balance.

3.3 Temperature interseasonal variability

3.3.1 Seasonal dependence of trend and anomalies

In the previous section we have concluded that a considerable warming occurred in the 0–200 m layer during the past 40 years (up to 0.28 °C/decade in the BoByClim analysis). This warming was even faster during the last 20 years (0.36 °C/decade in the ECOOP analysis). Besides, the warming trend fluctuates seasonally. Indeed, from the ECOOP analysis, the monthly trends over the period 1986-2005 range from 0.14 °C/decade in December to 0.61 °C/decade in June (not shown). Consistently, the BoByClim temperature at 5 m indicates the trends are lower during autumn and winter than during spring and summer (Fig. 10a). More precisely, the in situ data lead to an almost zero-trend during autumn (October to December) and a maximum trend during spring (April to June, ~0.6 °C/decade). Thus, the trend seasonal variations are slightly in advance of phase with respect to the temperature seasonal cycle, increasing the duration of the cool and warm periods ("de-seasonalisation", Fontán et al. 2008).

The temperature trend decreases with depth for each season, with a minimum in autumn at 50 m and a maximum in winter at 25 m. Below 100 m, a depth which roughly corresponds to the deepest extension of the surface mixed layer in winter, the trends are comparable at all seasons. Hence, at 100 m the trends range from 0.23 °C/decade in autumn to 0.38 °C/decade in summer. At 200 m, all seasonal trends are very close to their annual average, about 0.3 °C/decade.

Yearly anomalies also occur at preferential seasons (Fig. 10b). In the analyses of the ECOOP SST and of the temperature at 5 m from BoByClim, interseasonal anomalies are

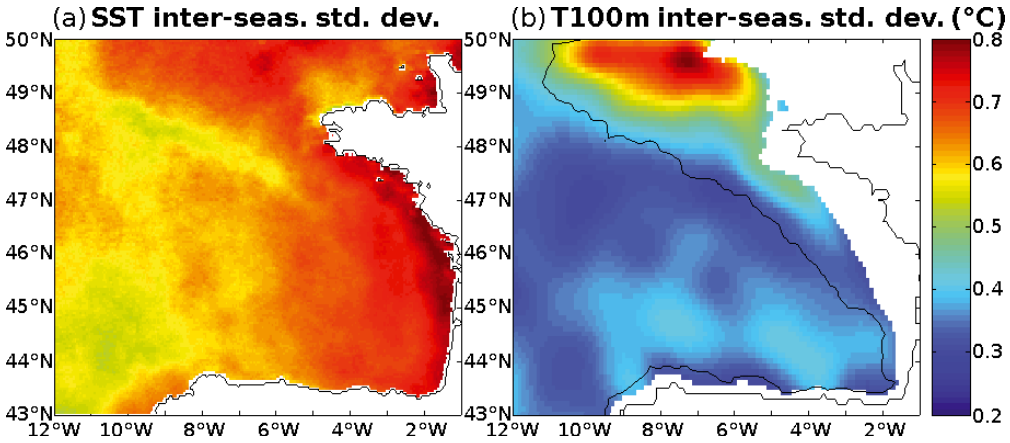

Fig. 11. Temperature interseasonal standard deviation, computed after removing the mean seasonal cycle (years 1986 to 2005): (a) ECOOP SST, (b) BoByClim temperature at 100 m. Black contour in (b): 200-m isobath.

weaker during winter (std. dev. = 0.35 °C). This was expected, as the mixed layer reaches its deepest extension in winter, when atmospheric perturbations are integrated over a thicker water column and produce moderate temperature variations. In contrast, during summer the mixed layer is very thin; thus, meteorological events can modify dramatically its temperature. Consequently, the interseasonal anomalies are highest during summer in the SST analysis (not shown). From the in situ temperature at 5 m, the standard deviation is slightly higher in spring than in summer. Indeed, the 5-m level is more sensitive to interannual changes in the mixed layer thickness, whose variations are highest during spring (restratification period).

The standard deviation of seasonal anomalies quickly decreases with depth, except in winter, when it remains close to its low surface value. Below 80 m, the interseasonal variability shows approximately the same value for each season. For instance, at 100 m, the standard deviation ranges between 0.28 °C and 0.31 °C. At 200 m, the interseasonal variability is about 0.25 °C for all seasons, very close to the interannual variability (0.20 °C). Thus, as for the long-term trend, the seasonal dependence of interannual anomalies is strong in the mixed layer and negligible below (on average, at depths greater than 100 m).

3.3.2 Geographic distribution of seasonal anomalies

The interseasonal temperature variability is obtained by removing the mean seasonal cycle at each point. In the ECOOP SST analysis (Fig. 11a), its overall amplitude is significantly higher than that of the interannual variability (std. dev. = 0.56 °C, instead of 0.40 °C) and its horizontal distribution differs notably (Fig. 7c). Indeed, the interseasonal variability is high over the northern Armorican shelf, but the highest values are found along the French coasts, apart from northern Brittany. The latter areas are also characterised by a strong seasonal cycle (not shown), largely dominating the temperature variability (std. dev. = 2.66 °C). Indeed, in areas where the seasonal cycle is strong, the inter-seasonal anomalies are potentially larger. The interseasonal variability is also low where the seasonal cycle is weak: along the Celtic and Armorican slopes, just to the north-west of Brittany and offshore the northwestern coast of Galicia. All three areas are characterised by intense mixing, due respectively to internal waves, tidal currents or slope currents. This mixing deepens the mixed layer and integrates the surface flux changes over a thicker water column, thus reducing seasonal variations.

At 100-m depth (Fig. 11b), the inter-seasonal variability is still higher than the interannual variability on average over the area (std. dev. = 0.34 °C, instead of 0.15 °C). The interseasonal variability is generally weaker at 100 m than at the surface, except over the western Armorican shelf, where it appears much stronger than elsewhere (exceeding 0.8 °C). Its spatial distribution is radically different from that of the seasonal cycle (not shown), which exhibits a high amplitude along the Celtic and Armorican slopes and a low amplitude in the southeastern corner. Overall, the surface temperature is essentially governed by the seasonal cycle, whereas interannual variability emerges with increasing depth.

3.3.3 Exceptional seasonal anomalies

A seasonal anomaly can be qualified as “exceptional” when its magnitude exceeds ± 1 standard deviation (Fontán et al. 2008). From the area averaged SST (Fig. 12a), the monthly anomalies often exceed the change associated with the 20-year trend (+0.7 °C). The coolest year is 1986, when the annual mean SST anomaly reaches –1.17 °C. This event is largely due to a very cool summer temperature, as the seasonal anomaly falls to –1.3 °C in July, and to a particularly cold winter temperature, as the seasonal anomaly reaches –0.6 °C in March. Conversely, SST is exceptionally high in 2003, mainly because of a very hot summer temperature, with a maximum seasonal anomaly of +1.4 °C in July. As noted previously, SST interseasonal variability is highest during summer. For instance, (i) 1997 is characterised by an exceptionally hot SST during summer, with a peak anomaly of +1.7 °C in September; (ii) in 1991, a very hot anomaly reaches +1.7 °C in August; and (iii) in 1993 a very cool anomaly is found during summer, with a peak in September (–1.2 °C).

At 100 m (Fig. 12b), the quarterly anomalies amplitude is comparable to the effect of the trend over 20 years (+0.6 °C).

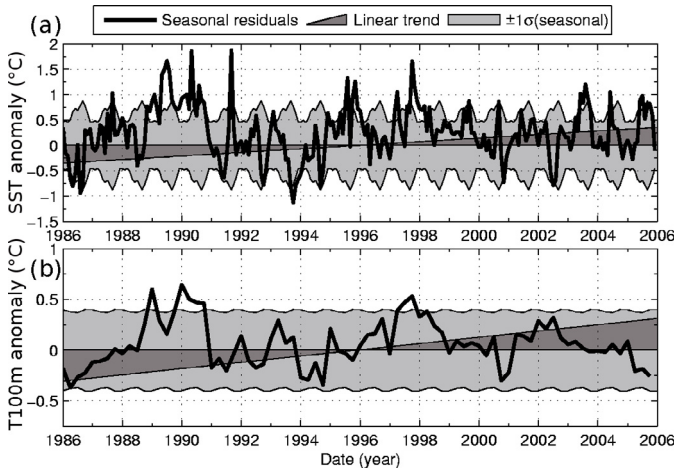

Fig. 12. Seasonal anomalies of temperature averaged horizontally over the study area. (a) Monthly anomalies from the ECOOP SST analysis. (b) Seasonal (quarterly) anomalies from BoByClim at 100 m. Grey area: average seasonal cycle of the std. dev. multiplied by ± 1. Values out of the grey area are called "exceptional" anomalies.

At this depth, interannual anomalies do not exhibit a preferred season (Fig. 10b). Most seasonal anomalies last for one or two quarters (examples in 1986, 1989, 1990, etc.), rarely during the whole year (except in 1991, 1997 and 2002). This contrasts strongly with the surface (Fig. 12a), where exceptional anomalies generally occur during summer (whether warm or cool) and rarely persist for more than one or two months. However, these surface events may induce sustained perturbations in the lower layers, through vertical advection and mixing.

4 Implications for the ecosystem and fishery

The results presented here on the temporal changes of temperature in the Bay of Biscay may have serious implications for the whole ecosystem and in particular for fishery resources. Climate change has been found to affect several biological and ecological processes from the scale of individual organisms to that of basin-wide processes (Stenseth et al. 2002).

Concerning megafauna, fishes and top predators, the results suggest that simplistic correlation analyses of the warming effect may not be relevant for several reasons: (i) the warming is not spatially homogeneous, (ii) annual anomalies during the study period are large compared to the trend, (iii) the warming is far from monotonous, with decreasing, steady and increasing periods occurring during the past 40 years (Fig. 3b, Fig. 6). At least in shallow waters, the average warming intensity was much smaller than the seasonal cycle, so that the physiological tolerance of adult fishes is unlikely to be affected. Nevertheless, fish recruitment has been shown to depend upon climatic effects (e.g. Stige et al. 2006) and the changes may affect other ecosystem components such as plankton (e.g. Miller and Harding 2007), whose modification could in turn impact higher trophic levels including exploited populations of fishes, molluscs and crustaceans. In addition to being complex and transmitted throughout the trophic web, climatic effects are combined with those of fishing, so that ascribing observed changes in exploited populations and communities to one or the other is not straightforward (Benoit and Swain 2008; Brander et al. 2007; Hsieh 2008).

In the study area, the estimated changes are not uniform in space and time. In particular, the Southern Celtic Sea appears to have warmed much more than the Southern Bay of Biscay during 1986-2005 (Fig. 7a,b). Previous studies concluded that the southern Bay of Biscay underwent stronger warming from the 1970s to the 1990s (Planque 2003; Koutsikopoulos et al. 1998). Planque et al. (2003) analysed SST data from Météo France over 1971-1998 and from the Comprehensive Ocean-Atmosphere Data Set (COADS) over 1844-2000. Based upon COADS, they found an overall warming of more than 1 °C over the past century and, based upon Météo France data, they found that the warming reached 0.6 °C per decade in the southern Bay of Biscay from 1971 to 1998. The difference in the spatial distribution of the warming might come primarily from different time periods: 1971-98 for Planque et al. (2003) vs. 1986-2005 in the present study. Also, the spatial resolution was higher in our study (0.044°) than in the data used by these authors (averaged of records from vessels, buoys and satellites over 0.5° × 0.5° cells). Nevertheless, the spatial distribution of warming and (probably to a lesser extent in our time interval) cooling might have varied over time. Thus, ecological studies should only rely upon estimates of temperatures relevant to their area and period, without any spatio-temporal extrapolation. The seasonal aspect might also be essential as, for example, the recent (1986-2005) warming was stronger in spring (Fig. 10), when the plankton blooms and the spawning of most fishes and other megafauna occurs. Lastly, the 3D analysis provided by BoByClim might allow better appraisal of the conditions experienced by biological populations than the 2D sea surface temperature previously available.

In the Bay of Biscay, some observed or modelled changes in the geographical distribution of species and communities have been ascribed to the recent warming. Quéro et al. (1998) observed the northward spread of a few sub-tropical fish species. Increase in the abundance of boarfish (*Capros aper*) and changes in the species composition of the demersal fish community were correlated to warming (Blanchard and Vandermeirsch 2005; Poulard and Blanchard 2005). Changes of flatfish species abundance, both increase and decrease, seem to have been driven by the effect of seawater warming (estimated from SST) on recruitment (Hermant et al. 2009). However, the distributions of eight abundant demersal fish species were not found to vary with changes in bottom temperature recorded during the same bottom trawl surveys (Persohn et al. 2009). The latter finding suggests that during the studied season (autumn) and time period (1992-2006), the adults and juveniles of the studied species were not sensitive to the observed range of temperature variation. Lastly, in the pelagic realm, anchovy (*Engraulis encrasicolus*) and, to a lesser extent, sardine (*Sardina pilchardus*) spawning habitats were shown to be mainly related to temperature conditions (Planque et al. 2007). At the larger spatial scale of the North Atlantic, Beaugrand et al. (2002) showed that changes in the species composition of calanoid copepods were correlated to large-scale hydroclimatic processes. No firm conclusion can be drawn from the Beaugrand et al. study regarding the Bay

of Biscay, because no time series of calanoid copepods was available in the Bay. Nevertheless, changes in copepod and other zooplankton are known to impact higher trophic levels (Beaugrand et al. 2003). These results can be regarded as a regional example of the complexity of interactions between hydrological conditions and biological populations and communities.

Understanding the full picture is a challenging task because the current ability to model and predict regional and global fish production is still poor. Moreover, the formulation of testable hypotheses and the investigations of probably complex interactions between organisation levels are only beginning (Brander 2007; Rijnsdorp et al. 2009). Lastly, although the main focus of marine ecologists has been climate warming, other climate factors including wind, freshwater runoff and acidification (Fabry et al. 2008; Le Pape et al. 2003; Planque and Buffaz 2008; Rijnsdorp et al. 2009) may affect populations and communities directly or indirectly. Their direct effect can be studied through temperature and salinity climatology and climate modelling (as in the present study). In addition, these tools may be indicators of other hydrological factors and might allow further research on the bio-ecological consequences of environmental variations at different levels of integration, from individual species to ecosystem compartments or trophic levels.

5 Conclusion

The temperature variations in the upper layer (0–200 m) of the Bay of Biscay have been described over the past 40 years, in terms of decadal trends, interannual variations and seasonal anomalies, with a spatial resolution of a few kilometres.

The 3D ocean model enables investigating the sources of temperature variability. In the upper layer, the air-sea fluxes primarily control the variability (std. dev. = 3.0 TW). However, when considering the whole 0–200 m layer, oceanic processes contribute largely to such variability and even dominate in some areas. In particular, the total transport (associated with horizontal and vertical currents) represents considerable sources (or sinks) of heat into (or out of) the domain (std. dev. = 1.6 TW). As a consequence, the heat transport through any of the three lateral boundaries of the studied domain exhibits interannual variations (std. dev. ~ 9 TW) much larger than those of the air-sea heat flux. It appears therefore that ocean currents can drive considerable changes of temperature in some areas and layers. An enormous amount of heat is brought into the Bay of Biscay by the North Atlantic Drift (mean = +22 TW). Although most of this heat is evacuated by currents toward the south and north (mean = –14 and –4 TW respectively), a significant part remains in the horizontal domain (mean = +4 TW). Almost all this excess heat is then transported downwards by vertical currents, heating deeper layers of the Bay of Biscay. Therefore, upper ocean currents not only impact temperature in the mixed layer, but also indirectly control temperature changes in the underlying water masses. Note that the details of the thermal balance depend on the domain lateral boundaries and depth, but its qualitative features remain unchanged when shifting the limits (Michel et al. 2009).

The Bay of Biscay temperature followed the evolution observed over the whole North Atlantic: a marked cooling until the mid 1970s, then a sustained warming over the next 30 years, which tends to accelerate during the 1990s (Levitus et al. 2005). In this particular region, the warming phase started 2–3 years earlier at the surface than at the 200-m depth. In addition, the warming phase is modulated by large oscillations, with a typical period of 6–7 years (similar to those of the NAO). The amplitude of year-to-year anomalies decreases rapidly with depth, while the warming rate culminates at about 50 m and decreases more slowly in deeper layers. As a consequence, from the 50-m depth and below, the temperature variations associated with the decadal trend over 10 years (0.28 °C/decade at 50 m) becomes higher than the interannual fluctuations (yearly residuals std. dev. = 0.26 °C at 50 m).

At the sea surface, the warming and interannual anomalies are stronger in the northern part, over the Armorican and Celtic shelves. The warming would be even stronger further north, over the English Channel (Saulquin and Gohin 2009). High interannual variability is also found at all depths (for instance, at 100 m) in the same regions, although its magnitude is generally weaker than close to the surface. The main mode of interannual variability in the upper 200 m seems to be related to the NAO, but this link probably undergoes seasonal fluctuations and would require more detailed studies to be confirmed.

The annual anomalies affecting the whole domain are generally localised in depth and time: their core lie in a specific layer, not always at the surface; their duration is generally limited to one or two seasons, not a full year. Moreover, the vertical extent of anomalies ranges from a few tens of meters to more than 200 m. The downward penetration of surface-generated perturbations on some occasions persists for several years. A seasonal dependence of trend and interannual anomalies has been illustrated: the trend is higher during summer and spring; the deviations from the seasonal cycle are weaker during winter. This dependence is most marked at the surface but also exists in the whole mixed layer. Below 50 m on average, the interannual variability is only slightly dependent on seasons.

These temperature changes might impact the ecosystem and the distribution of fisheries resources. In addition, they interact with the effect of fishing in a complex way. Research in this area is ongoing worldwide, and the accurate climatology of the Bay of Biscay might allow for progress in understanding changes at the regional scale.

Acknowledgements. We wish to thank the NODC/NOAA for providing the temperature analysis from the World Ocean Database. We also thank the DRAKKAR project team, especially Anne-Marie Treguier (CNRS, LPO, Brest), for providing us with outputs of the ORCA simulation. The ORCA025-G70 simulation was carried out by Jean-Marc Molines (CNRS, LEGI, Grenoble) with the computing resources of the IDRIS CNRS centre (Orsay, France). We are grateful to Francis Gohin and Bertrand Saulquin (DYNECO, Ifremer, Brest) for providing the ECOOP analysis of satellite SST, as well as fruitful discussions. We thank the SHOM for having authorised us to use their data within the framework of this study. We express sincere gratitude to the SISMER team (IDM, Ifremer, Brest) for their special contribution with regard to the BoByClim data, in particular Armel Bonnat for the digitalisation of historic data and Michèle Fichaut for the

data collection. We thank the CORIOLIS project, especially Fabienne Gaillard and Emmanuelle Autret, for supplying the optimal analysis program. Finally, we thank Serge Garcia and an anonymous reviewer for helping us in improving this manuscript in a stimulating way. This work was funded by a grant from Agence Nationale de la Recherche (ANR), through the CHALOUPE project.

APPENDIX

List of the websites from which observational or model data were used:

- WOD global analysis of interannual temperature change from 1955 to 2003 (Levitus et al. 2005): http://www.nodc.noaa.gov/OC5/DATA_ANALYSIS/heat_intro.html
- BoByClim monthly climatology of temperature in the Bay of Biscay: http://w3.ifremer.fr/climatologie-gascogne/index.php
- ECOOP interannual daily analysis of SST in the IBIROOS area from 1986 to 2006 (Saulquin and Gohin 2009): ftp://www.ifremer.fr/pub/ifremer/cersat/products/gridded/sst-l4hr-AVHRR-fnd/
- ORCA global simulation of ocean variability from 1958 to 2004 (Barnier et al. 2006): http://www.ifremer.fr/lpo/drakkar/index.htm
- NAO monthly index from 1950 to nowadays provided by the Climate Prediction Center: http://www.cpc.noaa.gov/data/teledoc/nao.shtml

References

Barnier B., et al., 2006, Impact of partial steps and momentum advection schemes in a global ocean circulation model at eddy permitting resolution. Ocean Dyn. 56, 543–567.

Benoit H.P., Swain D.P., 2008, Impacts of environmental change and direct and indirect harvesting effects on the dynamics of a marine fish community. Can. J. Fish. Aquat. Sci. 65, 2088–2104.

Beaugrand G., Reid P.C., Ibañez F., Lindlay J.A., Edwards M., 2002, Reorganization of North Atlantic marine copepod biodiversity and climate. Science 296, 1692–1694.

Beaugrand G., Brander K.M., Lindley J.A., Souissi S., Reid P.C., 2003, Plankton effect on cod recruitment in the North Sea. Nature 426, 661–664.

Blanchard F., Vandermeirsch F., 2005, Warming and exponential abundance increase of the subtropical fish *Capros aper* in the Bay of Biscay (1973-2002). C. R. Biol. 328, 505–509. doi:10.1016/j.crvi.2004.12.006

Brander K.M., 2007, Global fish production and climate change. Proc. Natl. Acad. Sci. USA 104, 19709–19714.

Brodeau L., Barnier B., Treguier A.M., Penduff T., 2007, Comparing sea surface atmospheric variables from ERA40 and CORE with a focus on global net heat flux. Flux News, newsletter of the WCRP workgroup on surface fluxes, 6-8 January 2007.

Curry R., Mauritzen C., 2005, Dilution of the northern North Atlantic Ocean in recent decades. Science 308, 1772–1774.

Fabry V.J., Seibel B.A., Feely R.A., Orr J.C., 2008, Impacts of ocean acidification on marine fauna and ecosystem processes. ICES J. Mar. Sci. 65, 414–432.

Fontán A., Valencia V., Borja A., Goikoetxea N., 2008, Oceanometeorological conditions and coupling in the southeastern Bay of Biscay, for the period 2001–2005: A comparison with the past two decades. J. Mar. Syst. 72, 167–177.

Friocourt Y., Levier B., Speich S., Blanke,B., Drijfhout S.S., 2007, A regional numerical ocean model of the circulation in the Bay of Biscay. J. Geophys. Res. 112, C09008.

Hermant M., Lobry J., Bonhommeau S., Poulard J.-C., Le Pape O., 2009, Impact of warming on abundance and occurrence of flatfish populations in the Bay of Biscay (France). J. Sea Res. 62.

Hsieh C.H., Reiss C.S., Hewitt R.P., Sugihara G., 2008, Spatial analysis shows that fishing enhances the climatic sensitivity of marine fishes. Can. J. Fish. Aquat. Sci. 65, 947–961.

Ivchenko V.O., Wells N.C., Aleynik D.L., 2006, Anomaly of heat content in the northern Atlantic in the last 7 years: Is the ocean warming or cooling? Geophys. Res. Lett. 33.

Knight J.R., Allan R.J., Folland C.K., Vellinga M., Mann M.E., 2005, A signature of persistent natural thermohaline circulation cycles in observed climate. Geophys. Res. Lett. 32.

Koutsikopoulos C., Beillois P., Leroy C., Taillefer F., 1998, Temporal trends and spatial structures of the sea surface temperature in the Bay of Biscay. Oceanol. Acta 21, 335–344.

Large W.G., 2007, CORE forcing for coupled ocean and sea-ice models. Flux News, newsletter of the WCRP workgroup on surface fluxes, 2-3 January 2007.

Le Pape O., Chauvet F., Désaunay Y., Guérault D., 2003, Relationship between interannual variations of the river plume and the extent of nursery grounds for the common sole (*Solea solea* L.) in Vilaine Bay. Effects on recruitment variability. J. Sea Res. 50, 177–185.

Levitus S., Antonov J., Boyer T., 2005, Warming of the World Ocean: 1955-2003. Geophys. Res. Lett. 32, L02604.

Lozier M.S., Leadbetter S., Williams R.G., Roussenov V., Reed M.S.C., Moore N.J., 2008, The spatial pattern and mechanisms of heat-content change in the North Atlantic. Science 319, 800–803.

Michel S., Treguier A.M., Vandermeirsch F., 2009, Temperature variability in the Bay of Biscay during the past 40 years, from an in situ analysis and a 3D global simulation. Cont. Shelf Res. 29, 1070–1087.

Miller W.D., Harding L.W. Jr., 2007, Climate forcing of the spring bloom in Chesapeake Bay. Mar. Ecol. Prog. Ser. 331, 11–22.

Persohn C., Lorance P., Trenkel V.M., 2009, Habitat preferences of selected demersal fish species in the Bay of Biscay and Celtic Sea, North-East Atlantic. Fish. Oceanogr. 18, 268–285.

Planque B., Beillois P., Jégou A.M., Lazure P., Petitgas P., Puillat I., 2003, Large-scale hydroclimatic variability in the Bay of Biscay: the 1990's in the context of interdecadal changes. ICES Mar. Sci. Symp. 219, 61–70.

Planque B., Bellier E., Lazure P., 2007, Modelling potential spawning habitat of sardine (*Sardina pilchardus*) and anchovy (*Engraulis encrasicolus*) in the Bay of Biscay. Fish. Oceanogr. 16, 16–30.

Planque B., Buffaz L., 2008, Quantile regression models for fish recruitment environment relationships: four case studies. Mar. Ecol.-Prog. Ser. 357, 213–223.

Poulard J.C., Blanchard F., 2005, The impact of climate change on the fish community structure of the eastern continental shelf of the Bay of Biscay. ICES J. Mar. Sci. 62, 1436–1443.

Quéro J.C., Du Buit M.H., Vayne J.J., 1998, Les observations de poissons tropicaux et le réchauffement des eaux dans l' Atlantique européen. Oceanol. Acta 21, 345–351.

Rijnsdorp A., Peck M.A., Engelhard G.H., Möllmann C., Pinnegar J.K., 2009, Resolving the effect of climate change on fish populations. ICES J. Mar. Sci. 66, 1570–1583.

Saulquin B., Gohin F., 2009, Mean seasonal cycle and evolution of the sea surface temperature from satellite and in situ data in the English Channel for the period 1985-2006. Int. J. Remote Sensing.

Stenseth N.C., Mysterud A., Ottersen G., Hurrell, J.W., Chan K-S., Lima M., 2002, Ecological effects of climate fluctuations. Science 297, 1292–1296.

Stige L.C., Ottersen G., Brander K., Chan K.-S., Stenseth N.C., 2006, Cod and climate: effect of the North Atlantic Oscillation on recruitment in the North Atlantic. Mar Ecol. Prog. Ser. 325, 227–241.

Vandermeirsch F., Charraudeau M., Bonnat A., Fichaut M., Maillard C., Gaillard F., Autret E., 2008, Bay of Biscay's temperature and salinity climatology. XI International Symposium on Oceanography of the Bay of Biscay, 1-4 April 2008, San Sebastian.